Title

Disorder-induced room temperature ferromagnetism in glassy chromites.

Journal

Scientific reports, 4(1)

ISSN

2045-2322

Authors

Araujo, C Moyses

Nagar, Sandeep

Ramzan, Muhammad

et al.

Publication Date

2014-04-01

DOI

10.1038/srep04686

Peer reviewed

SCIENTIFIC REPORTS

OPEN

SUBJECT AREAS:
PHYSICS
CONDENSED-MATTER PHYSICS

Received
15 October 2013

Accepted
26 March 2014

Published
15 April 2014

Correspondence and requests for materials should be addressed to K.V.R. (rao@kth.se)

Disorder-induced Room Temperature Ferromagnetism in Glassy Chromites

C. Moyses Araujo[1], Sandeep Nagar[2], Muhammad Ramzan[1], R. Shukla[3], O. D. Jayakumar[3], A. K. Tyagi[3], Yi-Sheng Liu[4,5], Jeng-Lung Chen[4,5], Per-Anders Glans[4], Chinglin Chang[5], Andreas Blomqvist[1], Raquel Lizárraga[6], Erik Holmström[6], Lyubov Belova[2], Jinghua Guo[4], Rajeev Ahuja[1,7] & K. V. Rao[2]

[1]Condensed Matter Theory Group, Department of Physics and Astronomy, Uppsala University, Box 516, SE-75120, Uppsala, Sweden, [2]Department of Materials Science, Tmfy-MSE, Royal Institute of Technology, SE100 44 Stockholm, Sweden, [3]Solid State Chemistry Section, Chemistry Division, Bhabha Atomic Research Centre, Mumbai, 400085 India, [4]Advanced Light Source, Lawrence Berkeley National Laboratory, Berkeley CA94720, USA, [5]Department of Physics, Tamkang University, Tamsui, Taiwan 250, R.O.C, [6]Instituto de Ciencias Físicas y Matemáticas, Facultad de Ciencias, Universidad Austral de Chile, Casilla 567, Valdivia, Chile, [7]Applied Materials Physics, Department of Materials and Engineering, Royal Institute of Technology (KTH), SE-100 44 Stockholm, Sweden.

We report an unusual robust ferromagnetic order above room temperature upon amorphization of perovskite [$YCrO_3$] in pulsed laser deposited thin films. This is contrary to the usual expected formation of a spin glass magnetic state in the resulting disordered structure. To understand the underlying physics of this phenomenon, we combine advanced spectroscopic techniques and first-principles calculations. We find that the observed order-disorder transformation is accompanied by an insulator-metal transition arising from a wide distribution of Cr-O-Cr bond angles and the consequent metallization through free carriers. Similar results also found in $YbCrO_3$-films suggest that the observed phenomenon is more general and should, in principle, apply to a wider range of oxide systems. The ability to tailor ferromagnetic order above room temperature in oxide materials opens up many possibilities for novel technological applications of this counter intuitive effect.

Tailoring multifunctional physical-chemical properties of oxide thin films represents a growing, and challenging area of interest in materials science[1]. Search for multiferroic materials with co-existing room temperature ferromagnetism and ferroelectricity is another area of intense research activity today for developing devices that can be controlled by both magnetic and electric potentials[2]. Ability to stabilize oxides into a glassy state gives rise to many technologically relevant properties thus enabling a wide range of applications in electronics, ranging from gate dielectrics in CMOS devices to flash memories[1–5]. The glassy state differs from the crystalline ground state of a material in the way the atoms are arranged. Since many physical properties of solids, in particular magnetism, are closely related to the local atomic structure, it is of fundamental interest to unveil the underlying effects of amorphization on the magnetic structure of a material.

Magnetic oxides provide a rich variety of fascinating phenomena and among them the perovskites have recently attracted special attention due to the possible coupling between their electrical and magnetic properties leading to novel multifunctional materials[6,7]. Normally, in amorphous magnetic oxides, random distribution of magnetic ions affects the antiferromagnetic (AFM) superexchange interactions, which usually dominate in these oxides and causes frustration in the arrangement of the spins[8–11]. This induces a spin glass transition and a drastic suppression of the magnetic ordering temperature[12,13]. $BiFeO_3$ is an example of such situation. In the crystalline state, $BiFeO_3$ is antiferromagnetic, with a Neel temperature of 643 K[14], whereas in the amorphous state, the material exhibits a transition from a paramagnetic to a spin glass state at 20 K[13].

Here, we report a drastic deviation from the above pattern. We find robust soft ferromagnetism above room temperature in amorphized $YCrO_3$-films obtained by Pulsed Laser deposition, while in contrast crystalline $YCrO_3$ is known to be an antiferromagnetic insulator with Neel temperature, $T_N \sim 140$ K. We have combined advanced spectroscopic techniques with first-principles calculations to reveal the underlying physics of this phenomenon. Such unusual transformation to ferromagnetism in amorphous oxides has been *reported* before[15] in amorphous $EuTiO_3$ with a $T_C = 5.5$ K while its crystalline phase was antiferromagnetic with $T_N = 5.3$ K.

The ability to tailor ferromagnetism above room temperature in oxide materials, induced by the disorder in the atomic lattice is a novel effect that deserves special attention and which might lead to many multifunctional technological applications.

Results

We have characterized the powder and the thin film by using X-ray diffraction (XRD), transmission electron microscopy (TEM), and a combined focused ion-beam (FIB)/scanning electron microscope (SEM). Figure 1(a) shows a typical film thickness determination from the focused ion-beam cross-section analysis, where the thickness of the film was found to be approximately 435 nm. In its powder and pellet forms, $YCrO_3$ is found to be crystalline (Figure 1b) with orthorhombic symmetry belonging to space group Pnma in close agreement with studies by Ramesha *et al.*[16]. Unlike the powder, the pulsed laser deposited (PLD) thin film does not show any XRD intensity peaks (see Figure 1b) and is consistent with an amorphous phase. The TEM analyses and electron diffraction pattern obtained (inset in Figure 1a) also confirms the amorphous structure for the thin films. It should also be pointed out that we have tried to crystallize the films to see if their properties are reversible by growing thicker films, or annealing the sample at high temperatures, without any success. The thicker films remained amorphous and on annealing at higher temperatures the film started deteriorating in structure and also in its magnetic properties probably because of possible effects of phase separations, which is an undesired outcome. Furthermore, we could not detect any signature of impurities in the samples within the detection limits from Energy Dispersive Spectroscopy (EDS), indicating that the observed ferromagnetism is intrinsic.

Figure 2(a) shows the field dependence, at 300 K, of the magnetization for a crystalline sample. As can be seen, the linear field dependence of the magnetization indicates a simple paramagnetic behavior at room temperature. Figure 2(b) displays the field sensitive temperature dependence of the magnetization measured at fields as low as 50 and 100 Gauss in both the zero field cooled (ZFC), and field cooled (FC) states. The sample undergoes a magnetic transition below about 140 K. On cooling down from room temperature in an external field of 2.5 kOe through the transition temperature down to 50 K, a minor hysteretic loop was found which does not close (as shown in Figure 2(c)). Furthermore, we find that the loop exhibits a high coercive field value that is dependent on the strength of the external field at which the sample was cooled, rate of cooling, and the lowest temperature reached. This phenomenon indicates that the crystal particles have strong anisotropy fields so that the maximum applied field was not enough to close the loop[17] resulting in the observed minor loop characteristics. In fact, at low temperatures the crystalline powder exhibits features, which may be related to the magnetic canting in the antiferromagnetic state.

For the thin film, amorphous phase, the scenario is different. The sample shows robust soft ferromagnetic behavior persisting to above 300 K with a finite low coercive field of about 29 Oe, as shown in Figure 2(d). In the crystalline form the super-exchange interaction between Cr atoms bridged by oxygen (Cr^{3+}-O^{2-}-Cr^{3+}) explains the antiferromagnetic ordering of Cr-spin-moments. However, a microscopic picture of the intrinsic structure of the amorphous phase remains to be understood to reveal the underlying physics of the room temperature ferromagnetic ordering.

It is important to note that although we have presented the properties of a 435 nm film as a representative amorphized film, we see similar results for films in the thickness range up to around 500 nm. Thicker films in the micron regime develop a mixed composite structure with the onset of partial crystallinity in them and the magnetic behavior is no longer that of a soft ferromagnet.

We investigated the electronic structure of the amorphous $YCrO_3$ by means of X-ray absorption spectroscopy (XAS) and

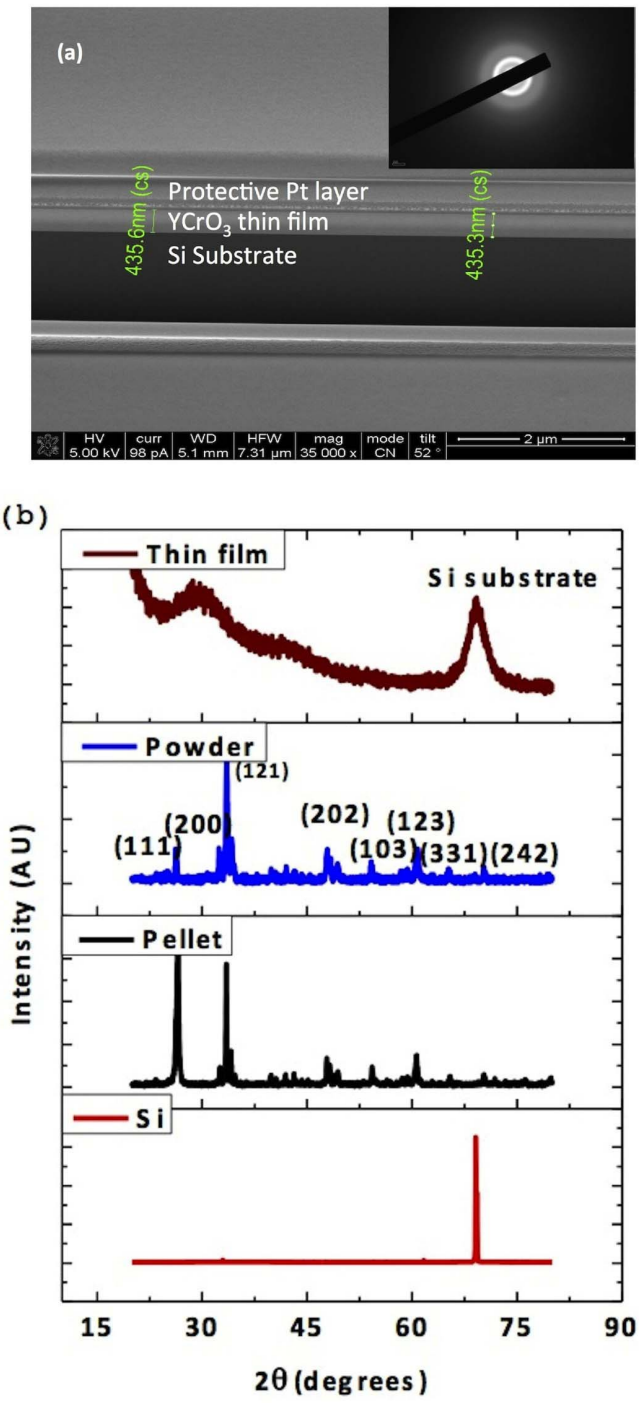

Figure 1 | Structural analysis. (a) Using Focused Ion-Beam assisted Scanning Electron Microscope; thickness of film was determined to be around 435.6 nm; (inset) TEM diffraction pattern of thin film shows a halo indicating complete amorphization. (b) XRD of $YCrO_3$ powder and pellet (used as target) shows orthorhombic crystal structure while the experimental radial distribution function for the thin film indicates only an amorphous phase on the silicon substrate.

X-ray emission spectroscopy (XES) on the beam line 8.0.1 at the Advanced Light Source at Berkeley Lab. The experimental setup is described in Ref. 18. Figure 3(a) shows the XAS spectrum of $YCrO_3$ at the oxygen *K*-edge. It was found that the oxidation state of Cr atoms in the bulk (100–200 nm in depth) obtained from the fluorescence yield (TFY) detection is Cr^{3+} with a small contribution of Cr^{4+} as indicated by the small peak at 529.2 eV. The

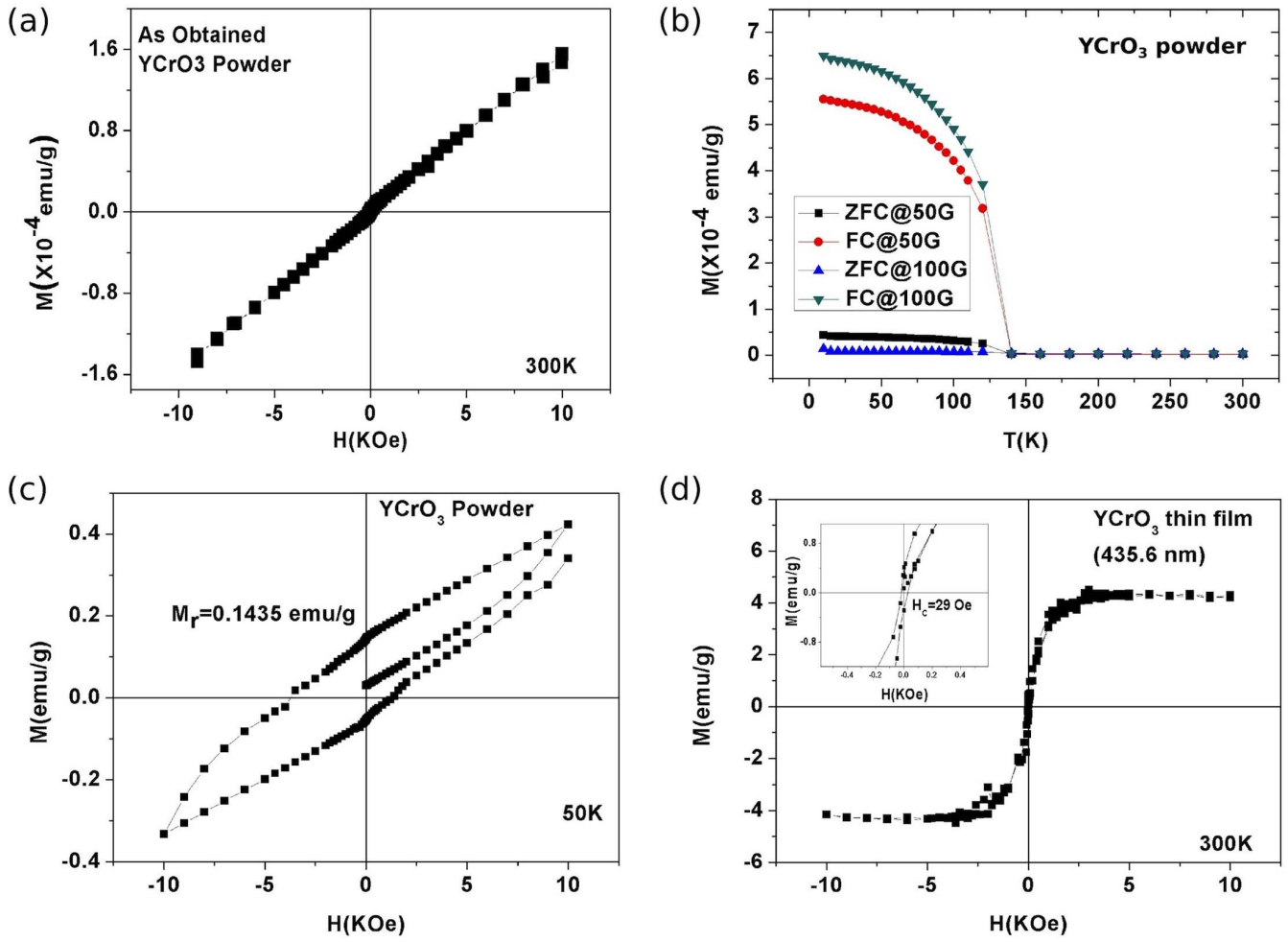

Figure 2 | Magnetization measurements. (a) Paramagnetic behavior of $YCrO_3$ powder at room temperature, (b) Temperature dependence of the magnetization for $YCrO_3$ powder showing Zero Field Cooled (ZFC) and Field Cooled (FC) curves measured at low fields, and the magnetic transition at 140°K, (c) the open minor hysteretic loop for the powder at 50 K upon field cooling from 300 K in an external field of 2.5kOe, and (d) the hysteretic loop for the amorphous thin film (435.6 nm) at 300 K showing robust ferromagnetism with magnetic coercivity, H_C = ~29 Oe (inset).

oxidation state of Cr on the surface at about 5–10 nm in depth that was resolved from total electron yield (TEY) detection is mainly Cr^{4+}.

In Figure 3 (b), we plot the oxygen bulk XES measurement together with XAS results from the surface as well as bulk in a standard *absorption-emission* spectrum[19,20]. The data show the metallic character for the amorphous phase. However, we have indicated in the figure that the band-gap may not be closed in the surface region. A similar *absorption-emission* spectrum (not shown here) clearly indicates a band-gap in our crystalline sample. Thus, the amorphization is accompanied by an insulator-metal transition. However, we are not able to explain the metallicity simply by the stabilization of mixed Cr^{3+} and Cr^{4+} valence states because we observed a similar mixed valence also in the insulating crystalline phase. Furthermore, such conducting behavior could be rigorously proved by measuring the transport properties. However, the spectroscopy measurements that we present in this work is considered to be sufficient to unveil the electronic structure information needed to interpret the observed magnetic phenomenon.

Figure 3(c) shows the XAS spectra of $YCrO_3$ at chromium *L*-edge. It further confirms that the oxidation state of Cr atoms in the bulk (100–200 nm in depth), also obtained from fluorescence yield (TFY) detection is Cr^{3+}, while the oxidation state at surface (5–10 nm in depth) detected from total electron yield (TEY) detection is Cr^{4+}.

Discussion

The results presented in Figures 2 and 3 indicate that the structural and electronic phase transitions of $YCrO_3$ are accompanied by a magnetic phase transition. In the crystalline structure, we have a super-exchange interaction mediated by bridging oxygen atoms favoring anti-ferromagnetic ordering, which is consistent with its insulating character. In the amorphous phase, local spin moments on Cr atoms may interact via double exchange, which is the dominant exchange mechanism in a mixed valence state (between surface Cr^{4+} and bulk Cr^{3+}) of metal ions. However, as we shall demonstrate later, this is only one of the contributions that may stabilize the ferromagnetic state near the surface region. In order to study further the nature of such magnetic and electronic transitions, we have also employed *ab initio* theory and the results will be presented in the following.

The calculations were carried out within the framework of density functional theory (DFT), as implemented in the VASP code (for more details see the methods section). We first investigated the electronic and magnetic properties of the ground-state crystalline structure of $YCrO_3$, which has orthorhombic symmetry belonging to space group *Pnma*. The calculated lattice parameters (a = 5.6 Å, b = 7.49 Å and c = 5.2 Å) compare well with our experimental findings (a = 5.52 Å, b = 7.53 Å and c = 5.24 Å) and also other results in the literature[21]. The system with AFM ordering is found to have a finite band-gap and is more stable than the system with FM ordering

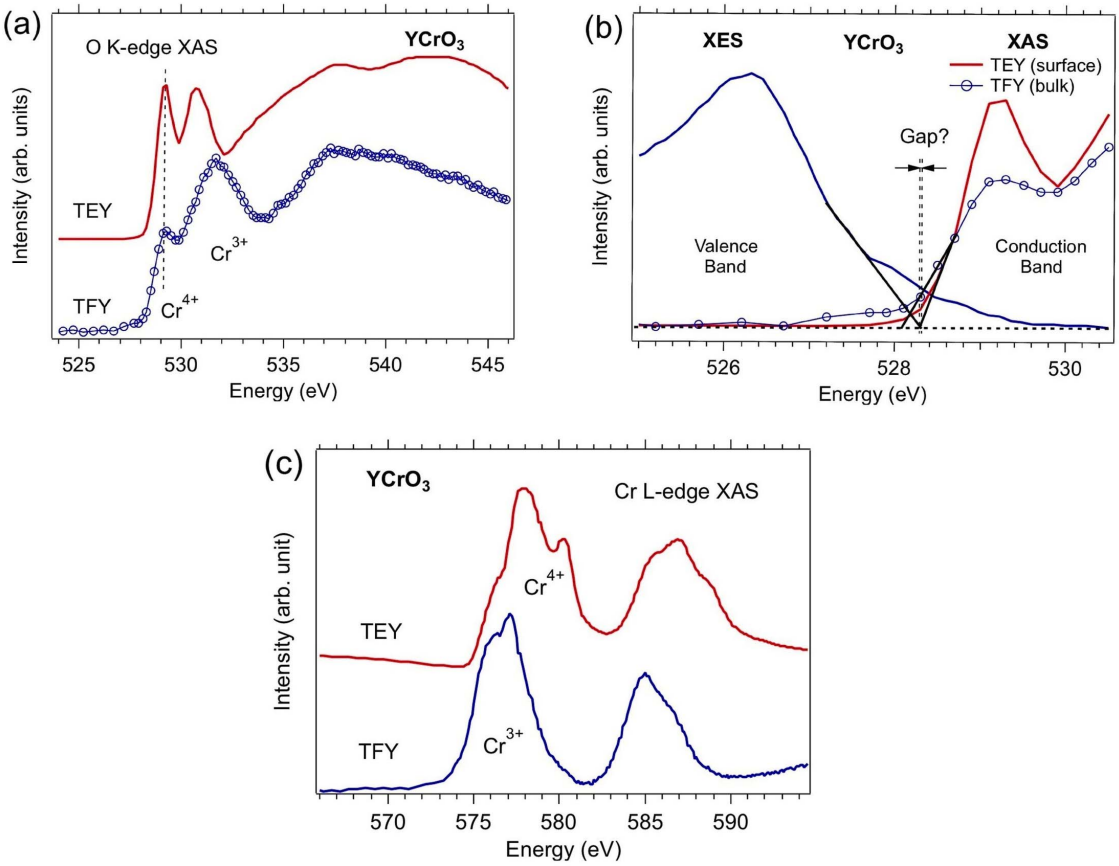

Figure 3 | **Spectroscopy measurements.** (a) O K-edge XAS; (b) O K-edge XES and XAS; the black lines are intended for identify the band issues; and (c) Cr L-edge XAS.

by 136 meV/unit cell. The local moment on Cr is found to be $3\mu_B$, which is consistent with the high-spin solution from Hund's rule for a d^3 configuration. In this system, the super-exchange interaction stabilizes the AFM state. This interaction is strongly dependent on the Cr-O-Cr bond angle, which is 146° for this orthorhombic cell. The calculated density of states for AFM ordering is shown in Figure 4(a).

To investigate the amorphous structure of $YCrO_3$, we have employed *ab inito* molecular dynamics (MD) simulations on a 160-atoms supercell, which was constructed from the meta-stable cubic perovskite structure[14]. The system was heated at 6000 K until it melted and lost memory of the initial structure. This was achieved after 10 ps of a MD run consisting of 10000 1 fs ionic steps. Careful analysis of the evolution of the radial distribution function and mean square displacement, not shown here for brevity, was performed at this point to ensure a liquid structure. Thereafter, we cooled down the system from 6000 to 300 K in 3 ps by means of a 3000 more MD time steps. The last snapshot of this simulation was then structurally optimized at 0 K to fully quench into the amorphous state.

To rule out the possibility that the choice of temperature parameters in the MD melt-quench procedure could influence the amorphous structure, we also performed some quenches directly from starting configurations with randomly placed atoms in the supercell by means of the stochastic quench (SQ) technique[22,23]. The SQ and MD generated structures have equivalent radial and angle distribution functions as well as partial coordination numbers, which indicate consistency in our amorphous structures[24].

The definition of the AFM state is ambiguous in the amorphous phase. The structural disorder will ensure an inescapable magnetic frustration that can result in a large set of almost degenerate magnetic configurations. Therefore a large number of different spin configurations with mixed parallel and anti-parallel alignments were calculated in the following protocol. First the system is fully optimized in the ferromagnetic state, with all spins polarized in the same direction. Then, we carried out a number of calculations with different initial magnetic arrangements, where no geometry optimization was performed. The local spins were allowed to relax but the total moment of the cell was kept fixed. In this way we could investigate the total energy change by varying only one degree of freedom and identify any tendency to prefer vanishing net moment in the cell. After that we successively allowed relaxation of the total spin and then the crystal geometry.

The outcome of this study was that the states with non-zero total magnetic moment in the supercell, that is, a ferromagnetic state, were systematically found to be the most energetically stable, indicating that the material should display partial FM ordering where some of the short-range interactions favor local AFM order. The average magnetic moment of Cr decreased to 2.5 μ_B in our most stable structures as compared to $3\mu_B$ in the crystal. Bader charge analysis[25–27] of the most stable structures showed that all Cr atoms are in the Cr^{3+} valence state, which is in good agreement with our XAS result for the bulk. The lowering of the average Cr moment was then found to be caused by a small set of magnetically frustrated Cr atoms in the low-spin state. The calculated FM order in absence of Cr^{4+} shows that the origin of the ferromagnetism in amorphous $YCrO_3$ cannot only be the mixed valence states. In the following we discuss the electronic structure and the changes in the Cr-O-Cr bond angles to explore other possible mechanisms.

The density of states of our lowest-energy amorphous structure is shown in Figure 4 (b). As can be seen, the system becomes metallic as no finite band gap is observed. To further understand the favoring of the FM state in the amorphous structure, we plot the Cr-O-Cr bond

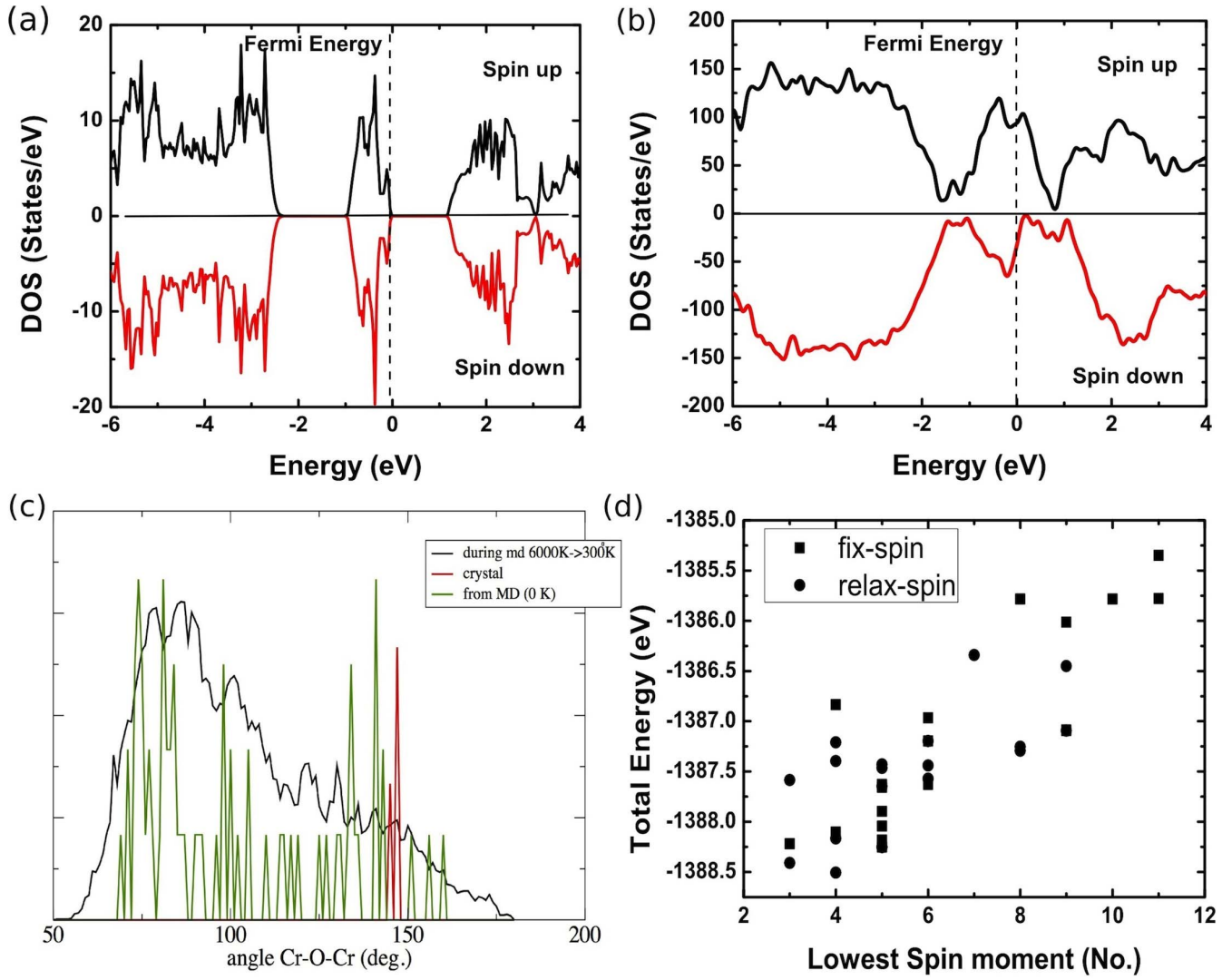

Figure 4 | Theoretical results. (a) Total DOS of crystalline phase, (b) Total DOS amorphous; (c) Cr-O-Cr bond angle distribution; and (d) total energy as a function of the number low spin states (local moment close to $1\mu_B$) on Cr atoms in the amorphous cell.

angle distributions of the amorphous and crystalline structures in Figure 4(c). We can see that the distribution of angles is very broad in the amorphous structure and that there are two main peaks. One peak is close to the Cr-O-Cr angle of the crystalline structure at 146°, meaning that this group of Cr pairs couple through the ideal AFM 180° superexchange mechanism. The other peak that is centered at 75° indicates that the interactions are closer to the ideal 90° FM superexchange over a large subsetset of Cr pairs. The metastable switching from AFM to FM as a function of Cr-O-Cr angle has been discussed by Ray *et al.*[21] connecting with phonon modes in the simple cubic perovskite structure.

The FM superexchange interaction occurs also in the half-metal CrO_2, with a Curie temperature of about 392 K[28], in which the double exchange is also claimed to be the driving force for the ferromagnetic ordering. In fact, the distinction between these two exchange mechanisms is not well defined. The double exchange is a combination of Coulomb and kinetic-exchange and therefore the FM superexchange can be considered as a double exchange mechanism. Besides that, as discussed above, our spectroscopy measurements indicate that mixed valence states occur near the surface region where the double exchange interaction is certainly contributing to FM ordering. Therefore, we believe that both superexchange and double exchange are responsible for the observed FM state.

To investigate the changes in the local moments in the amorphous state, we have counted the number of low spin moments of the Cr atoms in the supercell for the fixed-spin calculation and correlated this information with the total energy of the systems. As a result we have the graphic presented in Figure 4(d). As can be seen, the more low-spin moments, the higher is the total energy of the supercell, showing that the high-spin solution is energetically favored in the amorphous phase.

In summary, we report on the discovery of room temperature ferromagnetism in amorphous $YCrO_3$ thin films. Combining results from XAS, XES and first-principles calculations, we demonstrate that the amorphization affects the magnetic coupling between local spin-moments on Cr atoms. Bond angle disorder allows short range FM coupling, which percolates in the sample. In fact, our results indicate that the ferromagnetic ordering is a consequence of two exchange mechanisms, namely double exchange and FM superexchange. Furthermore, the high-spin solution for the local moments is energetically favored.

It should be emphasized again that disorder induced ferromagnetic ordering at room temperature leading to an electronic phase transition, is a counter-intuitive effect that might open up many possibilities for novel technological applications. Although we have used $YCrO_3$ as a case study, we have similar results on amorphizing $YbCrO_3$ and we believe our results are more general that would apply

for a wide range of antiferromagnetic oxides that become metallic in the amorphous phase.

Methods

Computational details. Density functional theory (DFT) calculations were performed using the PAW (Projector Augmented Wave) method[29] as implemented in the Vienna Ab initio Simulation Package (VASP)[30]. The PBE variant of the generalized gradient approximation (GGA) was used for the exchange-correlation functional[31]. The Kinetic energy cutoff of 600 eV and $5 \times 5 \times 5$ k-points mesh generated by the Monkhorst-Pack method were found suitable to achieve the total energy convergence within the accuracy of 0.005 eV. In the PAW potentials, the electronic states 4s, 4p, 5s, and 4d were treated as valence for Y, 3p, 3d and 4s states for Cr and 2s, 2p states for O. The convergence criterion for the electronic self-consistent cycle was fixed at 10^{-7} eV per cell and the forces on all ions were smaller than 10^{-5} eV/Å. Structural optimizations were performed by using a standard conjugate gradient method.

The synthesis methods. Since combustion reactions can yield large quantities of high quality powder, we used this method to produce enough powder for making a PLD target. Oxidants used in our work were Yttrium nitrate ($Y(NO_3)_3{\cdot}6H_2O$, 99.9%pure) and chromium nitrate ($Cr(NO_3)_3{\cdot}9H_2O$, 99.9% pure). Glycine (NH_2CH_2COOH) was used as fuel. These reactants were thoroughly mixed in the required molar ratios using a magnetic stirrer. Then the mixture was heated up till 100°C. On thermal dehydration a viscous liquid (gel) was formed. When this gel was further heated to ≈250°C, the viscous liquid swelled and auto-ignited, thus producing the powder which was calcinated at 600°C to obtain chemically pure and crystalline product. Due to a fuel-deficient ratio (1 : 0.5), the product was mainly $YCrO_4$. To obtain $YCrO_3$ the products were further heated at 800°C for 1 hour. The final powder was indexed on an.orthorhombic cell of $YbCrO_3$ with lattice parameters a = 5.193 Å, B = 5.491 Å and c = 7.481 Å. Using spark plasma sintering technique this powder was used to cast a 1″ diameter pellet which was 99% dense. Using this pellet as the target, homogeneous dense PLD thin films were deposited at a constant energy laser pulse rate of 150 mJ/pulse.

1. Greaves, G. N. & Sen, S. Inorganic glasses, glass-forming liquids and amorphizing solids. *Advances in Physics* **56**, 1–166 (2007).
2. Pal, B. N., Dhar, B. M., See, K. C. & Katz, H. E. Solution-deposited sodium beta-alumina gate dielectrics for low-voltage and transparent field-effect transistors. *Nature Mater.* **8**, 898–903 (2009).
3. Keszler, D. Oxide electronics transistors pick up steam. *Nature Mater.* **10**, 9–10 (2011).
4. Banger, K. K. *et al.* Low-temperature, high-performance solution-processed metal oxide thin-film transistors formed by a 'sol-gel on chip' process. *Nature Mater.* **10**, 45–50 (2011).
5. Taylor, M. P. *et al.* The remarkable thermal stability of amorphous In-Zn-O transparent conductors. *Adv. Funct. Mater.* **18**, 3169–3178 (2008).
6. Cheong, S. W. & Mostovoy, M. Multiferroics: a magnetic twist for ferroelectricity. *Nature Mater.* **6**, 13–20 (2007).
7. Goto, T., Kimura, T., Lawes, G., Ramirez, A. P. & Tokura, Y. Ferroelectricity and giant magnetocapacitance in perovskite rare-earth manganites. *Phys. Rev. Lett.* **92**, 257201 (2004).
8. Akamatsu, H., Tanaka, K., Fujita, K. & Murai, S. Spin dynamics in Fe_2O_3-TeO_2 glass: Experimental evidence for an amorphous oxide spin glass. *Phys. Rev. B* **74**, 012411 (2006).
9. Akamatsu, H., Tanaka, K., Fujita, K. & Murai, S. Spin dynamics in oxide glass of Fe_2O_3-Bi_2O_3-B_2O_3 system. *J. Magn. Magn. Mater.* **310**, 1506–1507 (2007).
10. Tanaka, K., Akamatsu, H., Nakashima, S. & Fujita, K. Magnetic properties of disordered oxides with iron and manganese ions. *J. Non-Cryst. Solids* **354**, 1347–1352 (2008).
11. Akamatsu, H., Oku, S., Fujita, K., Murai, S. & Tanaka, K. Magnetic properties of mixed-valence iron phosphate glasses. *Phys. Rev. B* **80**, 134408 (2009).
12. Lau, G. C., Klimczuk, T., Ronning, F., McQueen, T. M. & Cava, R. J. Magnetic properties of the garnet and glass forms of $Mn_3Al_2Si_3O_{12}$. *Phys. Rev. B* **80**, 214414 (2009).
13. Nakamura, S., Soeya, S., Ikeda, N. & Tanaka, M. Spin-glass behavior in amorphous $BiFeO_3$. *J. Appl. Phys.* **74**, 5652–5657 (1993).
14. Moreau, J. M., Michel, C., Gerson, R. & James, W. Ferroelectric $BiFeO_3$ x-ray and neutron diffraction study. *J. Phys. Chem. Solids* **32**, 1315 (1971).
15. Zong, Y., Kugimiya, K., Fujita, K., Akamatsu, H., Hirao, K. & Tanaka, K. Preparation and magnetic properties of amorphous $EuTiO_3$ thin films. *J. Non-Cryst. Solids* **356**, 2389–2392 (2010).
16. Ramesha, K., Llobet, A., Proffen, T., Serrao, C. R. & Rao, C. N. Observation of local non-centrosymmetry in weakly biferroic $YCrO_3$. *J. Phys.: Condens. Matter* **19**, 102202 (2007).
17. Khurshid, H., Li, W., Phan, M. H., Mukherjee, P., Hadjipanayis, G. C. & Srikanth, H. Surface spin disorder and exchange-bias in hollow maghemite nanoparticles. *Appl. Phys. Lett.* **101**, 022403 (2012).
18. Guo, J. H. & Nordgren, J. Resonant CK alpha X-ray emission of some carbon allotropes and organic compounds. *J. Electron Spectrosc. Relat. Phenom.* **110–111**, 1–13 (2000).
19. Dong, C. L. *et al.* Electronic structure of nanostructured ZnO from x-ray absorption and emission spectroscopy and the local density approximation. *Phys. Rev. B* **70**, 195325 (2004).
20. Guo, J. H. *et al.* Electronic structure of $YBa_2Cu_3O_x$ and $YBa_2Cu_4O_8$ studied by soft-x-ray absorption and emission spectroscopies. *Phys. Rev. B* **61**, 9140–9144 (2000).
21. Ray, N. & Waghmare, U. V. Coupling between magnetic ordering and structural instabilities in perovskite biferroics: a first-principles study. *Phys. Rev B* **77**, 134112-1-10 (2008).
22. Holmström, E. *et al.* Ab initio method for locating characteristic potential-energy minima of liquids. *Phys. Rev. B* **80**, 051111 (2009).
23. Holmström, E. *et al.* Structure discovery for metallic glasses using stochastic quenching. *Phys. Rev. B* **82**, 024203 (2010).
24. Lizárraga, R. *et al.* Structural characterization of amorphous $YCrO_3$ from first principles. *Europhys. Lett.* **99**, 57010 (2012).
25. Bader, R. F. W. *Atoms in Molecules: A Quantum Theory* (Clarendon Press, Oxford, 1990).
26. Henkelman, G., Arnaldsson, A. & Jonsson, H. A fast and robust algorithm for Bader decomposition of charge density. *Comput. Mater. Sci.* **36**, 354–360 (2006).
27. Sanville, E., Kenny, S. D., Smith, R. & Hankelman, G. Improved grid-based algorithm for Bader charge allocation. *J. Comp. Chem.* **28**, 899–908 (2007).
28. Coey, J. M. D. & Venkatesan, M. Half-metallic ferromagnetism: Example of CrO_2. *J. Appl. Phys.* **91**, 8345 (2002).
29. Blöchl, P. E. Projected augmented-wave method. *Phys. Rev. B* **50**, 17953–17979 (1994).
30. Kresse, G. & Furthmuller, J. Efficient iterative schemes for ab initio total-energy calculations using a plane-wave basis set. *Phys. Rev. B* **54**, 11169–11186 (1996).
31. Perdew, J. P., Burke, K. & Ernzerhof, M. Generalized gradient approximation made simple. *Phys. Rev. Lett.* **77**, 3865–3868 (1996).

Acknowledgments

It is a pleasure to thank Professor Mats Nygren at the Arrhenius labs, Stockholm University for his help in casting a 99% dense oxide target material made possible in his SPS facility. This research has been supported by the Swedish funding Agencies: VINNOVA, Hero-M Centre of Excellence at KTH, VR, STINT, Knut, Alice Wallenberg Foundation, Carl Tryggers Foundation and Swedish Energy Agency. The theoretical part of this work has used the resources provided by SNIC and UPPMAX. The Advanced Light Source is supported by the Director, Office of Science, Office of Basic Energy Sciences, of the U.S. Department of Energy under Contract No. DE-AC02-05CH11231. E.H. and R.L. acknowledge support from Chilean FONDECYT projects 1110602 and 1120334. M.R. acknowledges support from Higher Education Commission of Pakistan.

Author contributions

R.A. designed research, analyzed data and wrote the paper. C.M.A. and M.R. designed research, performed first-principles calculations, analyzed data and wrote the paper. A.B. performed first-principles calculations and analyzed data. R.L. and E.H. performed first-principles calculations, analyzed data and wrote the paper. S.N. performed film deposition, target preparation using SPS, structural and magnetic characterization. K.V.R. designed research, coordinated experimental work and wrote the paper. L.B. performed ion beam characterization. A.K.T. coordinated chemical synthesis technique and wrote the paper. R.S. and O.D.J. synthesized the chromites and produced the powder form for making the crystalline targets for PLD deposition. P.A.G., J.L., Y.S.L. and C.C. performed XPS, XAS spectral studies. J.G. performed XPS, XAS spectral studies and wrote the paper.

Additional information

Competing financial interests: The authors declare no competing financial interests.

How to cite this article: Araujo, C.M. *et al.* Disorder-induced Room Temperature Ferromagnetism in Glassy Chromites. *Sci. Rep.* **4**, 4686; DOI:10.1038/srep04686 (2014).